Gold Bull (2012) 45:197–201
DOI 10.1007/s13404-012-0068-3

ORIGINAL PAPER

Modulation of anisotropic middle layer on the plasmon couplings in sandwiched gold nanoshells

DaJian Wu · ShuMin Jiang · Ying Cheng · XiaoJun Liu

Published online: 10 October 2012

Abstract The influence of the spherical anisotropy (SA) of a middle layer on the plasmon resonance couplings in the sandwiched gold nanoshell (Au/SA/Au) has been investigated by means of a modified Mie theory. It is found that the plasmon couplings in the Au/SA/Au nanoshells are more sensitive to the permittivity along the radial direction of SA layer than the permittivity along the tangential direction. With increasing the anisotropic value of the middle layer, the dipole peaks of antisymmetric ω_-^- mode and symmetric ω_-^+ mode both show blue-shifts, while the shift of the antisymmetric ω_-^- mode is larger than that for the symmetric ω_-^+ mode. The larger anisotropic value of the SA layer induces the stronger near-field outside the nanoparticles for the antisymmetric ω_-^- mode, while the smaller anisotropic value makes the larger near-field for the symmetric ω_-^+ mode. We further have found that the middle SA layer with smaller anisotropic value is helpful to obtain larger electric fields inside the nanoshells, which may be useful for their potential applications in nonlinear optics.

Keywords Spherical anisotropy · Sandwiched gold nanoshells · Plasmon coupling · Near-field enhancement

Introduction

Metallodielectric layered nanoparticles and nanostructures have attracted increasing scientific and technological interest in recent years due to their importance in the fundamental physics and the potential applications in nanoelectronics, biomedical imaging, nano-optical device, and optical sensing [1–5]. A special interesting structure is metal–dielectric–metal three-layered nanoparticle, whose optical properties highly depend on the couplings between the plasmons of inner core and outer shell [6–8]. Changing the internal geometry of this nanoparticle not only shifts its resonance frequencies, but also strongly modifies the relative magnitudes of the absorption and scattering cross sections [5]. Mukherjee et al. [9] have found that an asymmetric core in $Au/SiO_2/Au$ can lead to an additional high multipolar Fano resonance. A significant superscattering phenomenon also has been found in the plasmonic–dielectric–plasmonic layered nanorod [3] and nanosphere [4].

Among the metallodielectric layered nanoparticles, the spherical anisotropic (SA) material–metal nano-composite shows a growing interest because of the applications in optical devices, surface-enhanced Raman spectroscopy (SERS) and optical nonlinearity enhancement [10–12]. Spherical anisotropy indicates that the tensor for dielectric function is radially anisotropic, i.e., the dielectric function is uniaxial in spherical coordinate with ε_r along the radial direction and ε_t along the tangential direction. Gao et al. [10] have reported that the adjustment of the dielectric anisotropy in the core or shell could result in large enhancements of the second harmonic generation and induced third harmonic generation susceptibilities at surface plasmon resonant frequencies. Yin et al. [11] have found that the introduction of spherical anisotropy into the core or the shell provides a novel approach to tailor the surface plasmon resonant frequencies and enhanced SERS peaks. It is further found that the spherically anisotropy of inner core can strongly modulate the Fano resonance in the Ag nanoshell with a spherically anisotropic core [12]. However, the modulation of spherical anisotropy on the plasmon couplings in metallodielectric layered nanoparticles is seldom reported.

D. Wu · Y. Cheng · X. Liu (✉)
School of Physics, Nanjing University,
Nanjing 210093, China
e-mail: liuxiaojun@nju.edu.cn

D. Wu · S. Jiang
Faculty of Science, Jiangsu University,
Zhenjiang 212013, China

In this paper, we have investigated the optical properties of the sandwiched gold nanoshell with an SA middle layer (Au/SA/Au) by using a modified Mie theory. Spherical anisotropy was indeed found in phospholipid vesicle systems [13] and in cell membranes containing mobile charges [14]. Lucas et al. [15] have easily established the spherically anisotropic materials by using the graphitic multishells. We focus on the influence of the spherical anisotropy of the middle layer on the plasmon couplings between the inner core and outer shell. In addition, the dependence of the local electric field enhancement on the spherical anisotropy of the middle layer has been further discussed in detail.

Electromagnetic scattering model

Figure 1 shows the specific geometry of a sandwiched gold nanoshell. The nanoparticle consists of a gold core with a radius of r_1, an SA middle layer with a radius of r_2, and a gold shell with a radius of r_3. The dielectric constant of embedding medium is ε_4. The SA middle layer is characterized by constitutive tensors of permittivity

$$\overleftrightarrow{\varepsilon_2} = \begin{pmatrix} \varepsilon_{2r} & 0 & 0 \\ 0 & \varepsilon_{2t} & 0 \\ 0 & 0 & \varepsilon_{2t} \end{pmatrix}. \tag{1}$$

ε_{2r} is along the radial direction and ε_{2t} is along the tangential direction. The dielectric functions of inner metal core ε_1 and outer metal shell ε_3 have real and imaginary frequency-dependent components, which are affected by the scattering of the conduction electrons in the particle surfaces. Thus, ε_1 and ε_3 are usually accounted by replacing the ideal Drude part in the dielectric function with a size-dependent one [8]. Light scattering by a spherical particle

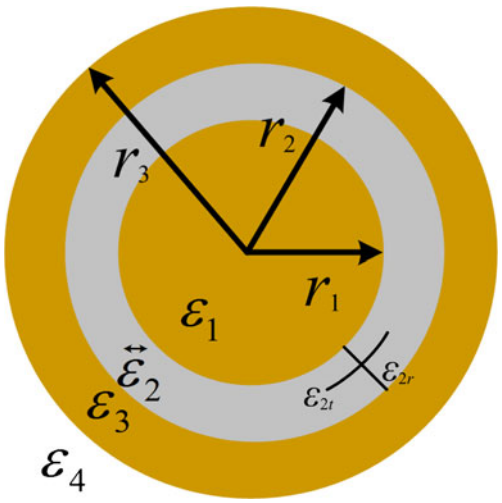

Fig. 1 Geometry diagram of a sandwiched gold nanoshell

can be expressed through Debye potentials [16]. For spherical anisotropic material, the electric ψ_{TM} and magnetic ψ_{TE} Debye potentials are presented as [17]

$$\frac{\varepsilon_r}{\varepsilon_t}\frac{\partial^2\psi_{TM}}{\partial r^2} + \frac{1}{r^2\sin\theta}\frac{\partial}{\partial\theta}\left(\sin\theta\frac{\partial\psi_{TM}}{\partial\theta}\right) + \frac{1}{r^2\sin^2\theta}\frac{\partial^2\psi_{TM}}{\partial\varphi^2} + k_0^2\varepsilon_r\mu_t\psi_{TM} = 0, \tag{2}$$

$$\frac{\mu_r}{\mu_t}\frac{\partial^2\psi_{TE}}{\partial r^2} + \frac{1}{r^2\sin\theta}\frac{\partial}{\partial\theta}\left(\sin\theta\frac{\partial\psi_{TE}}{\partial\theta}\right) + \frac{1}{r^2\sin^2\theta}\frac{\partial^2\psi_{TE}}{\partial\varphi^2} + k_0^2\varepsilon_t\mu_r\psi_{TE} = 0. \tag{3}$$

Here, $k_0 = 2\pi/\lambda$ is the wave vector in vacuum and $\mu_r = \mu_t = 1$. The electromagnetic waves are expanded to spherical partial waves using vector spherical harmonics, and then, Maxwell's boundary conditions are applied to resolve the unknown expansion coefficients of the scattered and interior waves. According to the Mie scattering theory, the obtained extinction efficiency Q_{ext}, scattering efficiency Q_{sca}, and absorption efficiency Q_{abs} can be expressed as [16]

$$Q_{ext} = \frac{2}{(k_4 r_3)^2}\sum_{n=1}^{\infty}(2n+1)\mathrm{Re}(a_n + b_n), \tag{4}$$

$$Q_{sca} = \frac{2}{(k_4 r_3)^2}\sum_{n=1}^{\infty}(2n+1)\left(|a_n|^2 + |b_n|^2\right), \tag{5}$$

$$Q_{abs} = Q_{ext} - Q_{sca}. \tag{6}$$

Here, $k_4 = k_0\sqrt{\varepsilon_4}$, a_n and b_n are the scattering coefficients. The information about spherical anisotropic middle layer is presented by the order of spherical Bessel functions [17]. The order can be expressed as

$$v = \left[n(n+1)\frac{\varepsilon_{2t}}{\varepsilon_{2r}} + \frac{1}{4}\right]^{1/2} - \frac{1}{2}. \tag{7}$$

Results and discussion

Figure 2a shows the extinction spectra of the Au/SA/Au nanoshells for the conditions of $\rho<1$. We assume ρ as the anisotropic value of the middle layer $\varepsilon_{2t}/\varepsilon_{2r}$. Here, r_1, r_2, and r_3 are fixed at 35, 50, and 65 nm, respectively. To discuss the influence of ε_{2r} on the plasmon resonances, ε_{2t} value is fixed at 2.04. The embedding medium is assumed to

be water (ε_4=1.7689). The plasmon resonances in the Au/SA/Au nanoshell can be considered as an interaction between the plasmons of a gold nanosphere and a gold nanoshell [5, 8, 18]. As shown in Fig. 2a, for $\varepsilon_{2t}/\varepsilon_{2r} = 1$, one dipole peak appears at 838 nm, which corresponds to the antisymmetric coupling (ω_-^- mode) between the plasmons of inner Au core (ω_s) and the symmetric mode of outer Au nanoshell (ω_-). Another dipole peak appears at 577 nm, which corresponds to the symmetric coupling (ω_-^+ mode) between ω_s and ω_- modes. The decreased ρ value means the increase of ε_{2r} value. With increasing ε_{2r} value, the dipole peak of ω_-^+ mode shows a red-shift from 577 nm at ρ=1 to 625 nm at ρ=1/5, while the dipole peak of ω_-^- mode shows a very large red-shift from 838 nm to 1,511 nm. The increased ε_{2r} value should decrease the induced charges in the inner and outer surfaces of the middle layer [19]. In this case, the plasmon resonance energies of ω_s and ω_- modes decrease, and hence, the red-shifts of the ω_-^- and ω_-^+ modes. According to plasmon hybridization theory [19–21], the ω_-^- mode is sensitive to the ω_- mode, while the ω_-^+ mode depends on the ω_s mode. The large red-shift of the ω_-^- mode indicates that the variation of ε_{2r} has more effect on the ω_- mode than the ω_s mode. Figure 2b shows the extinction spectra of the Au/SA/Au nanoshells for the conditions of ρ>1. Here, the ε_{2r} value is fixed at 2.04. The increased ρ value means the increase of ε_{2t} value. With increasing ε_{2t} value, the dipole peak of ω_-^+ mode shows a red-shift from 577 nm at ρ=1 to 611 nm at ρ=5, while the dipole peak of ω_-^- mode shows a red-shift from 838 to 859 nm. The small red-shifts of the ω_-^- and ω_-^+ modes suggest that the increased ε_{2t} value has little effect on the decrease of the induced charges in both surfaces of the middle layer. The red-shift of the mode is larger than that of the ω_-^- mode, which indicates the suppressed coupling between the ω_s and ω_- modes due to the increased ε_{2t} value.

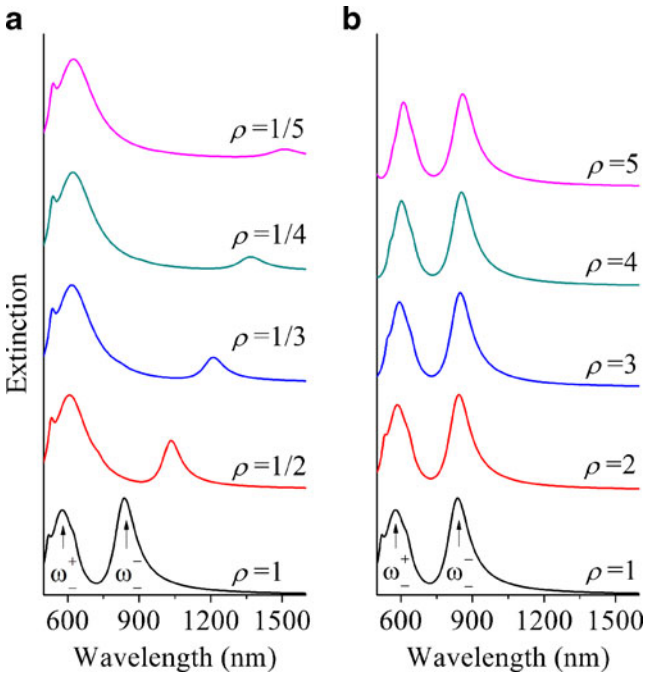

Fig. 2 Extinction spectra of the Au/SA/Au nanoshells with various anisotropic values of the middle layer for **a** $\varepsilon_{2t}/\varepsilon_{2r}$<1 and ε_{2t}=2.04 and **b** $\varepsilon_{2t}/\varepsilon_{2r}$>1 and ε_{2r}=2.04. Here, r_1, r_2, and r_3 are fixed at 35, 50, and 65 nm, respectively

Figure 3a, d shows the distributions of the electric field enhancement in the sandwiched nanoshell ($\omega_{2t}/\varepsilon_{2r}$=1) at wavelengths of 577 nm (ω_-^+) and 838 nm (ω_-^-), respectively. The distributions of the electric field enhancement show the typical dipole resonance properties [22]. The large electrical field on the shell occurs along the incident polarization and only locates within a few nanometer of the shell surface, while the inner core also exhibits a similar dipole pattern. In Fig. 3d, a large electric field is observed near the core mainly due to the antisymmetric coupling between the ω_s and ω_- modes, which leads to different kinds of charges induced in inner and outer surfaces of the middle layer [18]. Figure 3b, e shows the contour plots of the electric field enhancement in the Au/SA/Au with ρ=1/1.1 (divided by the results of the Au/SA/Au with ρ=1). The calculation wavelengths are fixed at 577 and 838 nm for subpanels b and e of Fig. 3, respectively. In Fig. 3b, the decrease of the induced charge in outer surface of the middle layer is larger than that in inner surface of the middle layer. For the ω_-^- mode, the increased ε_{2r} value induces the large electric field inside the nanoparticle. Figure 3c, f shows the contour plots of the electric field enhancement in the Au/SA/Au with ρ=1.1 at wavelengths of 577 and 838 nm (divided by the results of the Au/SA/Au with ρ=1), respectively. The increased ε_{2t} value should lead to the decrease of the induced charges on the inner and outer surfaces of the SA layer. It is obvious that the effects of the variation of ε_{2t} on the induced charges and the coupling between ω_s and ω_- modes are weaker than those due to the variation of ε_{2r}.

To further clarify the role of anisotropy, we keep the geometric average of dielectric components $\varepsilon_i = \varepsilon_{2r}/3 + 2\varepsilon_{3t}/3$ unchanged for the SA middle layer [12], while $\varepsilon_{2t}/\varepsilon_{2r}$ value is varied. Figure 4 shows the extinction spectra of the Au/SA/Au nanoshells with various ρ values. Here, r_1, r_2, and r_3 are fixed at 35, 50, and 65 nm, respectively. The ε_i value is fixed at 2.04. With an increasing ρ value, the dipole peak of the ω_-^- mode shows a distinct blue-shift from 1,589 nm at ρ=1/5 to 722 nm at ρ=5, while the strength of the peak increases. At the same time, the dipole peak of the ω_-^+ mode shows a blue-shift from 606 nm at ρ=1/5 to 503 nm at ρ=5, but the strength of the peak decreases. The influence of the variation of anisotropic value on the plasmon resonances in the Au/SA/Au nanoshell with ρ<1 is stronger than that for ρ>1. Figure 5a shows the dependences of the E-field enhancement in the Au/SA/Au nanoshell as a function of ρ value, which are calculated at the dipole resonance wavelengths of ω_-^+ mode. In Fig. 5a, the dashed

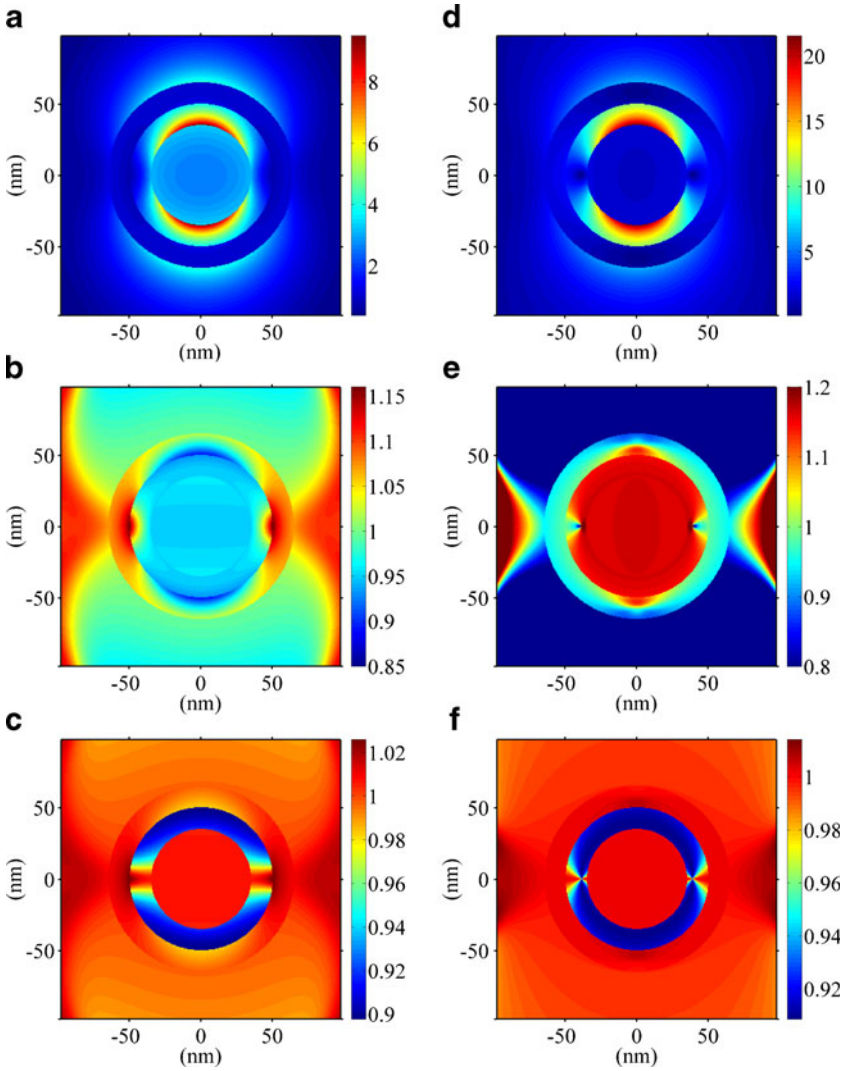

Fig. 3 Contour plots of the electric field enhancements in Au/SA/Au nanoshells with **a** ρ=1 (ε_{2r}=ε_{2t}=2.04) at 577 nm, **b** ρ=1/1.1 (ε_{2t}=2.04) at 577 nm, **c** ρ=1.1 (ε_{2r}=2.04) at 577 nm, **d** ρ=1 (ε_{2r}=ε_{2t}=2.04) at 838 nm, **e** ρ=1/1.1 (ε_{2t}=2.04) at 838 nm, and **f** ρ=1.1 (ε_{2r}=2.04) at 838 nm. Here, r_1, r_2, and r_3 are fixed at 35, 50, and 65 nm, respectively

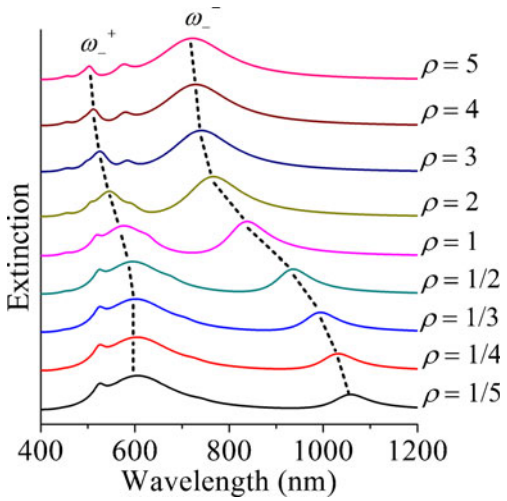

Fig. 4 Extinction spectra of the Au/SA/Au nanoshells with various ρ values (ε_i=2.04). Here, r_1, r_2, and r_3 are fixed at 35, 50, and 65 nm, respectively

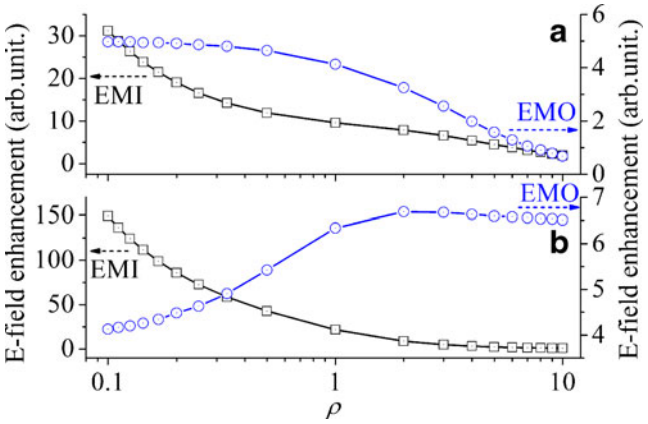

Fig. 5 Dependences of the E-field enhancement maximum for **a** ω_-^+ mode and **b** ω_-^- mode in Au/SA/Au nanoshells as a function of ρ value. Here, ε_i=2.04, r_1=35 nm, r_2=50 nm, and r_3=65 nm. The dashed circle line for right-hand scale and dashed square line for left-hand scale represent the variations of EMO and EMI, respectively

circle line for right-hand scale represents the variation of E-field enhancement maximum outside the nanoshell (EMO), which often locates on the outer surface of the particle and at the poles along the incident polarization. The dashed square line for left-hand scale shows the variation of the E-field enhancement maximum inside the nanoshell (EMI), which can be obtained on the surface of inner gold core and at the poles along the incident polarization. In Fig. 5b, the dashed circle line for right-hand scale and dashed square line for left-hand scale represent the variations of EMO and EMI, respectively, which are calculated at the dipole resonance wavelengths of ω_{-}^{-} mode. It is found with the increase in ρ value that the EMO for the ω_{-}^{+} mode decreases from 4.97 at ρ=1/10 to 0.68 at ρ=10, while the EMI decreases from 31.15 at ρ=1/10 to 1.92 at ρ=10. At the same time, the EMO for the ω_{-}^{-} mode increases first from 4.13 at ρ=1/10 to 6.68 at ρ=2 and then decreases to 6.51 at ρ=0, while the EMI decreases from 149.00 at ρ=1/10 to 0.85 at ρ=10. It is found that the smaller ρ value is helpful to obtain larger electric field inside the nanoparticle. The larger ρ value of the middle SA layer can induce the larger near-field outside the nanoparticle for the ω_{-}^{-} mode and the smaller ρ value makes larger near-field for the ω_{-}^{+} mode.

Conclusion

We have investigated the plasmon resonance properties of the Au/SA/Au nanoshells. The extinction spectra and the electric field enhancement of the Au/SA/Au nanoshells have been calculated based on a modified Mie scattering theory. We focus on the influence of the spherical anisotropy of the middle layer on the plasmon resonance couplings in the Au/SA/Au nanoshells. It is found that the permittivity along the radial direction plays a dominant role on the plasmon couplings in Au/SA/Au nanoshells, and the permittivity along the tangential direction leads to significant modulations. With the increase of ρ, both the dipole peaks of the ω_{-}^{-} and ω_{-}^{+} modes show blue-shifts. The variation of the ω_{-}^{-} mode is stronger than the ω_{-}^{+}mode. The large ρ value of the middle SA layer can induce the large near-field outside the nanoparticle for the ω_{-}^{-} mode and the small ρ value can induce the large near-field for the ω_{-}^{+} mode. Such enhanced near-field can be used to the enhanced Raman excitation and emission. Furthermore, the small ρ value is helpful to obtain larger electric field inside the nanoparticle, which may be helpful for their potential applications in nonlinear optics.

Acknowledgments This work was supported by the National Basic Research Program of China under grant no. 2012CB921504, the National Natural Science Foundation of China (11174113, 10904052, 11274171, 11104319, and 11204129), and project funded by the Priority Academic Program Development of Jiangsu Higher Education Institutions.

References

1. Hao F, Sonnefraud Y, Dorpe PV, Maier SA, Halas NJ, Nordlander P (2008) Symmetry breaking in plasmonic nanocavities: subradiant LSPR sensing and a tunable Fano resonance. Nano Lett 8:3983–3988
2. Kodali AK, Schulmerich MV, Palekar R, Llora X, Bhargava R (2010) Optimized nanospherical layered alternating metal-dielectric probes for optical sensing. Opt Express 18:23302–23313
3. Ruan ZC, Fan SH (2010) Superscattering of light from subwavelength nanostructures. Phys Rev Lett 105:013901
4. Ruan ZC, Fan SH (2011) Design of subwavelength superscattering nanospheres. Appl Phys Lett 98:043101
5. Bardhan R, Mukherjee S, Mirin NA, Levit SD, Nordlander P, Halas NJ (2010) Nanosphere-in-a-nanoshell: a simple nanomatryushka. J Phys Chem C 114:7378–7383
6. Xia XH, Liu Y, Backman V, Ameer GA (2006) Engineering sub-100 nm multi-layer nanoshells. Nanotechnology 17:5435–5440
7. Hu Y, Fleming RC, Drezek RA (2008) Optical properties of gold-silica-gold multilayer nanoshells. Opt Express 16:19579–19591
8. Wu DJ, Jiang SM, Liu XJ (2011) Tunable Fano resonances in three-layered bimetallic Au and Ag nanoshell. J Phys Chem C 115:23797–23801
9. Mukherjee S, Sobhani H, Lassiter JB, Bardhan R, Nordlander P, Halas NJ (2010) Fanoshells: nanoparticles with built-in Fano resonances. Nano Lett 10:2694–2701
10. Gao L, Yu XP (2007) Second- and third-harmonic generations for a nondilute suspension of coated particles with radial dielectric anisotropy. Eur Phys J B 55:403–409
11. Yin YD, Gao L, Qiu CW (2011) Electromagnetic theory of tunable SERS manipulated with spherical anisotropy in coated nanoparticles. J Phys Chem C 115:8893–8899
12. Wu DJ, Jiang SM, Liu XJ (2012) A tunable Fano resonance in silver nanoshell with a spherically anisotropic core. J Chem Phys 136:034502
13. Lange B, Aragon SR (1990) Mie scattering from thin anisotropic spherical shells. J Chem Phys 92:4643–4650
14. Ambjörnsson T, Mukhopadhyay G, Apell SP, Käll M (2006) Resonant coupling between localized plasmons and anisotropic molecular coatings in ellipsoidal metal nanoparticles. Phys Rev B 73:085412
15. Lucas AA, Henrard L, Lambin P (1994) Computation of the ultraviolet absorption and electron inelastic scattering cross section of multishell fullerenes. Phys Rev B 49:2888–2896
16. Bohren CF, Huffman DR (1983) Absorption and scattering of light by small particles. Wiley, New York
17. Luk'yanchuk BS, Qiu CW (2008) Enhanced scattering efficiencies in spherical particles with weakly dissipating anisotropic materials. Appl Phys A 92:773–776
18. Radloff C, Halas NJ (2004) Plasmonic properties of concentric nanoshells. Nano Lett 4:1323–1327
19. Prodan E, Lee A, Nordlander P (2002) The effect of a dielectric core and embedding medium on the polarizability of metallic nanoshells. Chem Phys Lett 360:325–332
20. Prodan E, Radloof C, Halas NJ, Nordlander P (2003) A hybridization model for the plasmon response of complex nanostructures. Science 302:419–422
21. Prodan E, Nordlander P (2004) Plasmon hybridization in spherical nanoparticles. J Chem Phys 120:5444–5454
22. Kelly KL, Coronado E, Zhao LL, Schatz GC (2003) The optical properties of metal nanoparticles: the influence of size, shape, and dielectric environment. J Phys Chem B 107:668–677